INSTITUTE OF PHYSICS PUBLISHING JOURNAL OF PHYSICS D: APPLIED PHYSICS

J. Phys. D: Appl. Phys. **38** (2005) 1649–1657 doi:10.1088/0022-3727/38/11/003

Axial and radial development of microdischarges of barrier discharges in N_2/O_2 mixtures at atmospheric pressure

R Brandenburg[1], H-E Wagner[1], A M Morozov[2] and K V Kozlov[2]

[1] Institute of Physics, Ernst-Moritz-Arndt University of Greifswald, Domstr. 10a, 17489 Greifswald, Germany

[2] Department of Chemistry, Moscow State University, Leninskie Gory 1, Str.3, 119899 Moscow, Russia

E-mail: wagner@physik.uni-greifswald.de

Received 16 December 2004, in final form 4 February 2005
Published 20 May 2005
Online at stacks.iop.org/JPhysD/38/1649

Abstract

Microdischarges (MDs) of filamentary barrier discharges (BDs) in air and N_2/O_2 gas mixtures at atmospheric pressure were investigated using the techniques of spatially resolved cross-correlation spectroscopy (CCS) and short exposure time photography (ICCD-camera). The BDs were generated in symmetric discharge cells (configuration of the type 'glass–glass') with two semi-spherical electrodes in order to localize the repetitive MDs at a fixed position. In the case of CCS measurements, the MD development was imaged through spatio-temporal distributions of the radiation intensity of the (0–0) transition of the 2nd positive system of molecular nitrogen ($\lambda = 337$ nm). Two-dimensional optical scanning of the MD channel (in the axial and radial directions of the MD) was carried out for a BD operated in a gas mixture consisting of 6 vol% O_2 and 94 vol% N_2. This gas composition had been found to provide the extremely high stability of the discharge that was necessary for the time-consuming scanning procedure. In the middle of the gap, the MD channel diameter was found to be about 0.3 mm and to expand towards both electrodes. With dielectrics, outward propagating discharges were observed. Short exposure time photos of the MDs taken using an ICCD-camera under the same experimental conditions as for the CCS measurements revealed a branched structure of these discharges on the surfaces, not only on the cathode but on the anode as well. The influence of voltage amplitude on the spatio-temporal distribution of individual MDs of a BD in air was investigated using the CCS-instrument operated in a so-called 'direct start–stop' mode which enabled statistical analysis of the MD sequences within a time range of about 30 μs.

1. Introduction

Barrier discharges (BDs) in air and in N_2/O_2 mixtures are known to consist of a multitude of microdischarges (MDs) [1, 2]. Due to their short duration a time-resolution in the subnanosecond range is needed. Their small dimensions require a spatial resolution in the submillimetre range. Furthermore, MDs appear statistically in time and in position. Thus, investigation of the spatio-temporal development of a MD is a challenge to plasma diagnostics, and it is not surprising that a great deal of effort has been devoted to computer simulation (e.g. [3,4]). The spectroscopic technique of spatially resolved cross-correlation spectroscopy (CCS) provides the necessary temporal resolution in a subnanosecond time scale. Furthermore, the high sensitivity of this method enables investigation of the weak light signals of MDs and a spatial scanning of this object in the submillimetre range. The CCS technique has been used to analyse the mechanism of MD development in air in a two-glass-sided, symmetric BD-cell with a discharge gap, g, of about 1.2 mm [5, 6]. These

investigations have been performed along the axis of the MD. Based on a kinetic model, important local plasma parameters were determined experimentally for the first time. It was shown that an ionizing wave starts near the surface of the anode and crosses the gap with an increasing velocity reaching $10^6\,\mathrm{m\,s^{-1}}$. The maximal electric field strength, E/n, of the ionizing wave grows from 120 Td at the anode up to 240 Td at the cathode, while the maximum of the electron density is located at the anode. In combination with current pulse measurements, the maximum electron density has been estimated to be of the order of $10^{12}\,\mathrm{cm^{-3}}$ [7]. Recently, systematic investigations of MDs in binary N_2/O_2 gas mixtures (oxygen content varied within the range 0.5–70 vol%) were carried out [8–10]. For the mixtures considered, the same characteristic features of the MD luminosity distributions as for air were observed for the selected spectral bands. These results allow us to conclude that the mechanism of the MD development does not change. However, the duration of the MD decay phase as well as the magnitude of the transferred charge decreases with an increase in oxygen content. These effects may be explained by collisional quenching of nitrogen excited species by oxygen molecules and by the dominant role of electron attachment. At oxygen concentrations below 0.05 vol%, the BD operates in the diffuse mode, provided that the driving voltage amplitude is sufficiently low. The spatio-temporal distributions of the light intensity correspond to the Townsend mechanism of discharge development [8].

In this contribution our axially and radially resolved CCS measurements are reported. Since CCS is a single-photon accumulation technique, a high reproducibility and long-time stability of the repetitive MDs are required. Systematic investigations of BDs in flowing binary gas mixtures of oxygen and nitrogen demonstrated a very good reproducibility and stability of MDs in working gases containing 3–6 vol% of O_2 in N_2 [8]. Therefore, axially and radially resolved measurements are carried out for a gas mixture 6 vol% O_2 + 94 vol% N_2; this gas composition had been found to provide the extremely high stability of the discharge that is necessary for the time-consuming scanning procedure. Since the development of the MD proceeds in a similar way in all binary gas mixtures of N_2 and O_2 considered in [8], the results for the above-mentioned mixture can be seen as being representative for the entire concentration range. The axially and radially resolved CCS measurements describe the MD development in the volume as well as on the dielectric surfaces. From these investigations detailed experimental data on the local plasma parameters (reduced electric field strength, electron density) of BDs in the volume as well as on the electrode surfaces can be expected. Additionally, the structure of the discharges on the surfaces and the dynamics of subsequent MDs are investigated. To investigate individual MDs, an ICCD-camera is used for short exposure time photography.

The plan of this paper is outlined as follows: a few important aspects of the experimental technique are considered in section 2, since a corresponding full and detailed description of the apparatus and procedure of the CCS measurements has been presented in previous papers [5, 6]. In section 3, the experimental results on the MD evolution are reported first (section 3.1), followed by a discussion of the ICCD-camera records, with special attention to the structure of the surface discharges (section 3.2). Finally, in section 3.3 the statistical behaviour of a sequence of subsequent MDs is discussed.

2. Experimental set-up

In this work, the same experimental equipment was used as described earlier (e.g. [5, 6]). In order to localize repetitive MDs, the BDs was generated between two semi-spherical electrodes, both covered by glass. The electrodes were mounted with a gap distance, g, within the range 0.9–2.2 mm (see figure 1). Furthermore, the electrode arrangement provided the possibility of observing not only the volume part of the MD but also the surface discharge processes. The discharge cell was placed in a vacuum chamber which was evacuated down to 0.1 mbar before each experiment. The working gas composition was obtained using mass-flow controllers (MKS 1259 CC), with the total gas flow rate maintained at about $40\,\mathrm{litre\,h^{-1}}$. The BD was driven by a sinusoidal voltage (frequency $f = 6.9\,\mathrm{kHz}$, peak-to-peak amplitude U_0 of about 12 kV). To investigate single MDs the voltage amplitude has been adjusted so as to maintain the discharge in a mode with only one MD per voltage half-period.

The technique of spatially resolved CCS and the experimental set-up have been described in detail, e.g. in [5, 6]. Here only a brief review is given. In figure 2 the CCS set-up is shown schematically. By means of a quartz lens, the discharge zone was imaged onto an optical slit. By appropriate adjustment and movement of this slit, the discharge area could be scanned in the vertical (r) and horizontal (z) directions (resolution not worse than 0.1 mm). The localized radiation (so-called 'main signal') was resolved

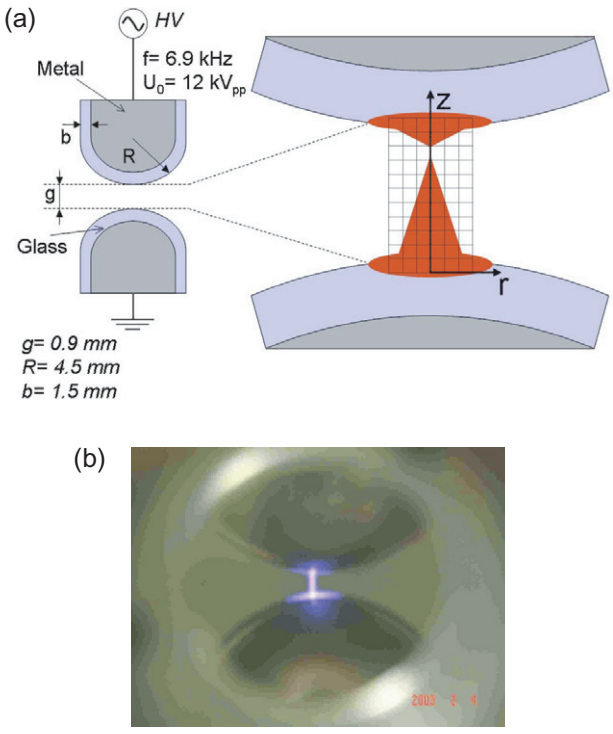

Figure 1. (*a*) Principal scheme of the discharge cell with indicated area of axial and radial optical scanning. (*b*) Photo of the discharge cell with the localized repetitive MDs.

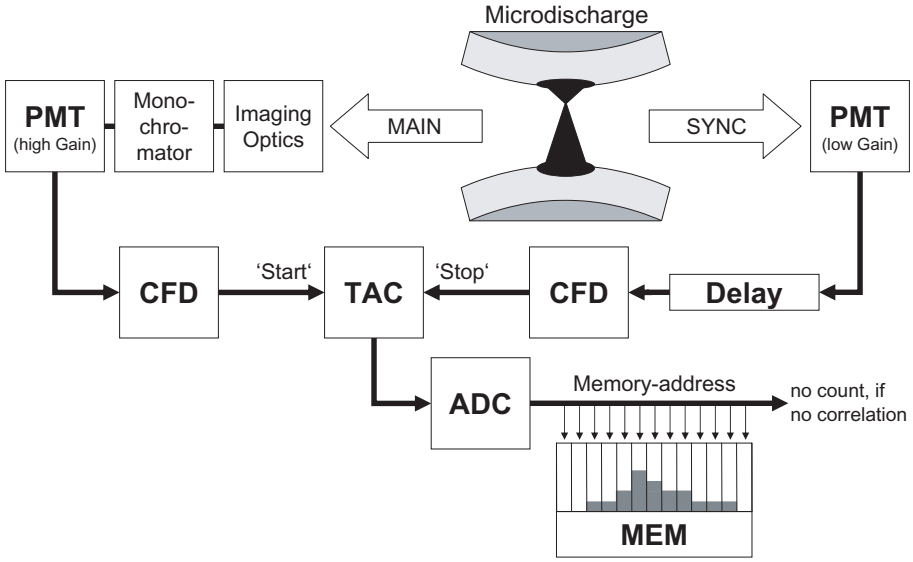

Figure 2. An outline of the CCS-apparatus and measurement procedure (the 'reversed start–stop' mode is shown). Abbreviations: PMT, photomultiplier; CFD, constant fraction discriminator; TAC, time-to-amplitude convertor; ADC, analogue-to-digital converter; MEM, memory.

spectrally using a monochromator (Triax 320, ISA Jobin Yvon). Monochromatic light was detected using the high-gain photomultiplier (PMT), which operated in a single photon counting mode (H5773-04, Hamamatsu). The second detector for the synchronizing ('sync') signal was adjusted so as to reach the maximal possible temporal resolution of the steep front of a light pulse, since the derivative of this signal was actually used to define a zero-point of the relative time scale (so-called optical triggering procedure). Measurements of the correlation functions and accumulation of the results were carried out using a time correlated single photon counting (TC-SPC) board (SPC-530, Becker and Hickl GmbH). The basic components of the TC-SPC instrument are two constant fraction discriminators (CFD), a time-to-amplitude converter (TAC), an analogue-to-digital converter (ADC) and a memory (MEM). The discriminators are used to select electric pulses which belong to a pre-defined range of amplitudes. A selected pulse of the main signal initiates a linear rise in the voltage of the TAC, and the first pulse following the selected pulse of the sync signal stops this rise. The value of the measured quantity (voltage amplitude) is converted to the number of the corresponding time channel of the device (actually, to a memory address) by the ADC and the number of counts of the addressed MEM-channel is increased by one. The entire scale of a memory segment consists of 1024 channels. If no synchronizing signal comes and the voltage of the TAC reaches its upper limit, then no count is registered in the MEM-segments. A correspondence between the time value and the number of the time channel is determined by the duration of the voltage rise, which is variable from 50 ns to several microseconds. A shift in the zero-point to the left over the time axis is possible due to the insertion of the coaxial delay-cable between the detector for the sync signal and the TC-SPC module. Typically, up to 10^7 counts were accumulated in the memory segment with a maximal count rate for a measurement of 5 min duration. The temporally resolved intensity distribution was recorded with a time resolution of about 0.1 ns. Additionally the MEM-segments are controlled by a pattern generator (PPG-530, Becker and Hickl GmbH) in order to resolve the measurements along the phase of the applied voltage (not shown in figure 2).

The CCS technique can be performed in two different modes. In the case described above, the main signal starts the TAC and the sync signal stops it. This mode is referred to as 'reversed start–stop'. The CCS results discussed in section 3.1 were obtained using the CCS apparatus at the University of Greifswald (Germany) described above as well as in [5, 6, 11]. It is operated in the 'reversed start–stop' mode. The results in section 3.3 correspond to the CCS measurements in the 'direct start–stop' procedure (TS-SPC module 'Fluor 99', NPO Spektroskopiya, [11]) which were used with the CCS set-up at the Moscow State University (Russia). Since this set-up is actually rather similar in design and posseses comparable technical characteristics, it is not necessary to describe it in further detail here.

Besides CCS, an ICCD-camera (PI-MAX, Princeton Instruments) for short exposure time photography was used. ICCD pictures have been taken from the MD-channel (side view) as well as from the dielectric surfaces, for which the discharge cell was turned by approximately 30° towards the camera. While CCS gives an averaged result (over many repetitive MDs) due to the accumulation of measurement data, the ICCD-camera records light emitted by an individual MD. The exposure time (gate of 15 μs) was adjusted so as to prevent any overlapping of the MDs following one another while maximizing the probability of their detection.

3. Results and discussion

3.1. Microdischarge development

Under the conditions being considered, the emission spectrum of the BD consists of the molecular bands of nitrogen, namely the second positive system (SPS) and the first negative system (FNS). Both radiating species, $N_2(C\,^3\Pi_u)$ and $N_2^+(B\,^2\Sigma_u^+)$, are

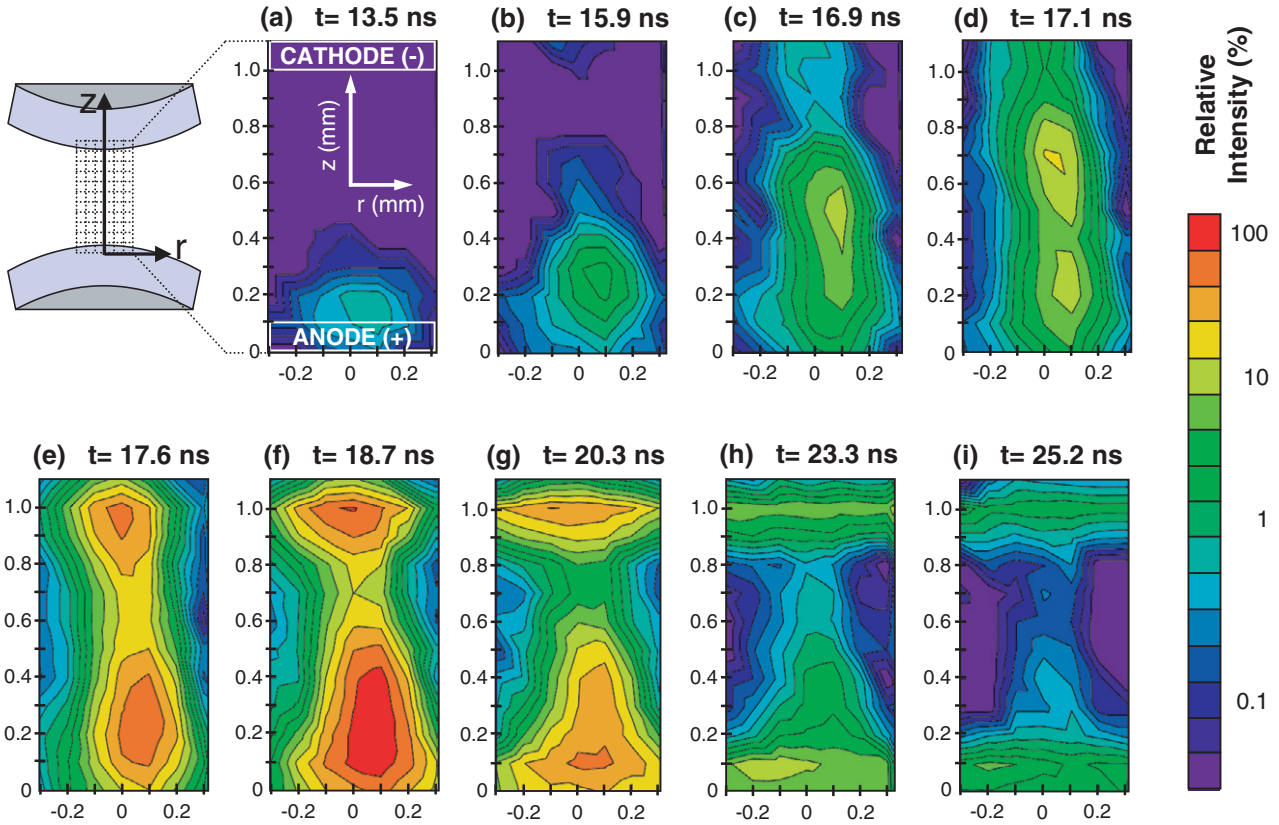

Figure 3. Evolution of the light intensity distributions for MDs in a mixture of N_2 (94 vol%) and O_2 (6 vol%) (SPS, (0–0) transition at 337 nm).

excited by direct electron impact (the corresponding values of excitation energy, E_C and E_B, for the vibrational level $\upsilon' = 0$ are indicated below):

$$N_2(C\,^3\Pi_u)_{\upsilon'} \rightarrow N_2(B\,^3\Pi_g)_{\upsilon''} + h\nu, \quad E_C = 11.0\,\text{eV}, \qquad (1)$$

$$N_2^+(B\,^2\Sigma_u^+)_{\upsilon'} \rightarrow N_2^+(X\,^2\Sigma_u^+)_{\upsilon''} + h\nu, \quad E_B = 18.7\,\text{eV}. \qquad (2)$$

For the $(\upsilon' - \upsilon'') = (0\text{–}0)$ transition of the SPS at $\lambda = 337$ nm, the evolution of the axially and radially resolved distributions of the MD luminosity (radiation intensity) is shown in figure 3. The results presented up to now are integrated measurements over the MD channel depth. Therefore, the local intensities can be somewhat modified. Nevertheless, from the results in figure 3 the following subsequent phases of MD development can be distinguished.

(1) The MD starts with a Townsend pre-breakdown phase (figure 3(*a*)), lasting for more than 150 ns [5]. At this time no significant space charge has been formed yet, and the maximum of light intensity is observed at the anode surface. It should be noted that the radial distribution of the intensity is not uniform. Only a small area of the dielectric is covered. The position of the MD seems to be determined by the residual charges on the dielectrics deposited in their predecessor.

(2) The light intensity at the anode increases in time (figure 3(*b*)). When a sufficient positive space charge has grown up in front of the anode, a cathode directed ionizing wave starts to propagate. The ionizing wave is caused by local distortion of the electric field and moves with an acceleration towards the cathode (figures 3(*c*)–(*e*)). At this time, the value of the MD channel diameter (i.e. the value of the FWHM of the radial intensity distribution) is about 0.3 mm. At the back of the ionizing wave, electrons drift towards the anode, generating a glow near the anode. Thus two light spots are clearly seen in figure 3(*e*). These spots correspond to two active zones of the MD with different properties: the region near the cathode is characterized by a higher electric field [5]. Additionally, our previous results [5] have indicated that the density of electrons near the cathode, in contrast, is smaller than at the anode. The maximum velocity of the cathode directed ionizing wave is about $v = 2 \times 10^6\,\text{m s}^{-1}$ under the experimental conditions being considered [8].

(3) The ionizing wave crosses the discharge gap within about 3 ns. At the same time when it reaches the cathode the anode glow has developed. At this stage of MD development charge carriers are accumulated on the electrodes much faster than during the previous phases. Therefore, the radial component of the electric field increases and causes considerable broadening of the MD channel at the electrodes. The values of the corresponding diameters on the surface become comparable with the discharge gap width (figure 3(*f*)).

(4) The MD decays within a period of about 10 ns (figures 3(*g*)–(*i*)) due to the reduction in axial electric field caused by accumulation of charge carriers on the dielectrics. This general decay is accompanied by propagation of the surface discharges.

To visualize the radial development of the MDs in more detail, the cross-sections, $I(r, t)_{z=\text{const}}$, of the experimental three-dimensionally arrays $I(z, r, t)$ are plotted below. These

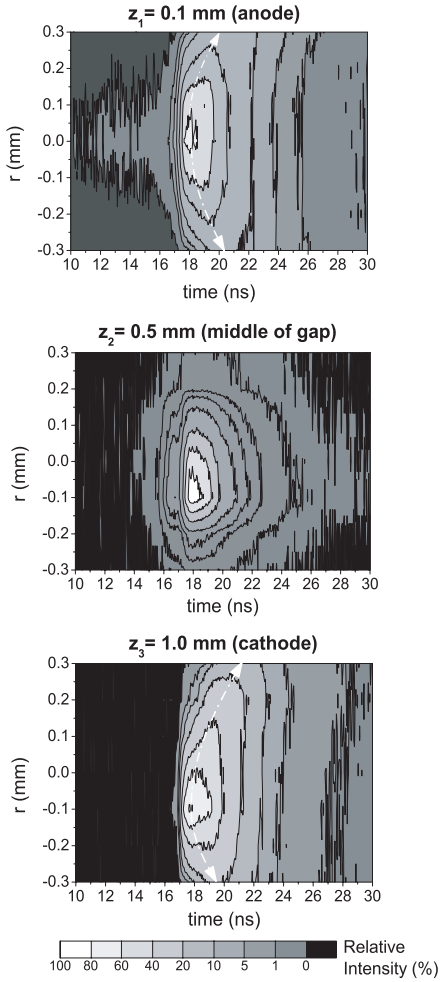

Figure 4. Radial intensity distributions for three different positions in the discharge gap ($z_1 = 0.1$ mm, at the anode; $z_2 = 0.5$ mm, in the middle of the gap; $z_3 = 1.0$ mm, at the cathode.)

intensity distributions are shown as functions of the radial position (r) and time (t) in figure 4 for three different positions (z_i) in the discharge gap.

On the dielectric surfaces ($z_1 = 0.1$ mm and $z_3 = 1.0$ mm), the MD channel is wider than in the middle of the gap ($z_2 = 0.5$ mm). Furthermore, during the decay phase of MD development (i.e. for $t \geqslant 17$ ns, see figure 4), the radial intensity distributions on the cathode as well as on the anode are broadening continuously. This effect may be attributed to discharges on the surface which propagate outwards from the MD axis. The movement of the local maxima of light intensity (i.e. the points $(r, t_{\max})$, where $t_{\max}$ corresponds to $I_{\max}(r) = \max\{I(r,t)\} = I(r, t_{\max}); \forall 0 < t < 50$ ns) on both electrodes is indicated by the white dash-dotted arrows in the plots for z_1 and z_3 in figure 4. This propagation occurs with a velocity of about 10^5 m s^{-1}, which is about one order of magnitude lower than the maximum velocity of the cathode directed ionizing wave. In the distribution at the anode ($z_1 = 0.1$ mm), the Townsend pre-breakdown phase is found for $t \leqslant 16$ ns, while at the cathode ($z_3 = 1.0$ mm) the registered light intensity within the same time period corresponds to the background level.

As discussed in the previous paper [8] in great detail, a variation of the oxygen content within the range 0.1 vol%–100 vol% does not cause any qualitative changes in the MD development mechanism, and it does not exert any noticeable influence on the velocity of the cathode directed ionizing wave. Thus in air, as a dilute gas, the same MD development can be expected. Due to collisional quenching of nitrogen excited species by oxygen molecules and the dominant role of electron attachment, a faster decay of the MD could be investigated in air.

The radiation kinetics for the SPS, (0–0) transition of a non-equilibrium plasma in nitrogen–oxygen mixtures at atmospheric pressure is determined by the elementary processes as discussed below [12–14].

- The excitation of the molecules of nitrogen (in the ground state) is dominated by direct electron impact (3):

$$e + \mathrm{N_2}(X\,^1\Sigma_g^+)_{\upsilon=0} \rightarrow \mathrm{N_2}(C\,^3\Pi_u)_{\upsilon'=0} + e. \qquad (3)$$

  Indirect processes such as stepwise excitation, processes including the vibrational kinetics or excitation via collisions of $\mathrm{N_2}(A\,^3\Sigma_u^+)$ metastable states, can be neglected for the conditions being considered. Due to the high density of nitrogen and oxygen molecules these excited states are quenched before they can undergo a second collision with an electron or another excited molecule.
- The decay of the excited state $\mathrm{N_2}(C\,^3\Pi_u)_{\upsilon'=0}$ is due to the spontaneous emission of the excited molecules (4) and the collisional quenching of the excited species by the molecules of nitrogen and oxygen (5). At the conditions being considered the latter is the dominating loss process:

$$\mathrm{N_2}(C\,^3\Pi_u)_{\upsilon'=0} \rightarrow \mathrm{N_2}(B\,^3\Pi_g)_{\upsilon''=0} + h\nu, \quad (\lambda_C = 337.1\ \mathrm{nm}), \qquad (4)$$

$$\mathrm{N_2}(C\,^3\Pi_u)_{\upsilon'=0} + \mathrm{N_2/O_2} \xrightarrow{K^C_{N_2}/K^C_{O_2}} \text{Products}. \qquad (5)$$

  Here $K^C_{N_2}$ and $K^C_{O_2}$ are the rate constants for collisional quenching of the state $\mathrm{N_2}(C\,^3\Pi_u)_{\upsilon'=0}$ by molecular nitrogen and oxygen, respectively.

Within the frame of the kinetic scheme (3)–(5), the local concentration of the excited species $\mathrm{N_2}(C\,^3\Pi_u)_{\upsilon'=0}$, denoted below as $n_C(r,t)$, obeys the following differential equation:

$$\frac{\mathrm{d}n_C(r,t)}{\mathrm{d}t} = k_C(E/n) n_{N_2} n_e(\vec{r},t) - \frac{n_C(\vec{r},t)}{\tau^C_{\mathrm{eff}}}. \qquad (6)$$

Here $k_C(E/n)$ is the rate constant of reaction (3). The densities of electrons, molecular nitrogen and oxygen in the ground electronic states are denoted as n_e, n_{N_2} and n_{O_2}, respectively. The effective lifetime, τ^C_{eff}, depends on the gas composition as well as the pressure and is defined as follows:

$$\frac{1}{\tau^C_{\mathrm{eff}}} = K^C_{N_2} n_{N_2} + K^C_{O_2} n_{O_2} + \frac{1}{\tau^C_0}. \qquad (7)$$

Here τ^C_0 is the radiative lifetime of the state $\mathrm{N_2}(C\,^3\Pi_u)_{\upsilon'=0}$ ($\tau^C_0 = 45$ ns). Since $K^C_{N_2} < K^C_{O_2}$, as the oxygen content gets higher the effective lifetime gets smaller. For the gas mixture 6 vol% O_2 + 94 vol% N_2 at atmospheric pressure one gets

$\tau_{\mathrm{eff}}^{\mathrm{C}} = 1.2$ ns (calculation based on the values of $K_{\mathrm{N_2}}^{\mathrm{C}}$ and $K_{\mathrm{O_2}}^{\mathrm{C}}$ taken from [15]).

The light intensities for the spectral bands of the SPS (0–0) transition, $I_{\mathrm{C}}(\vec{r}, t)$, calculated from the corresponding experimentally measured photon count rates are directly proportional to the rate of reaction (4). Therefore, equation (6) can be rewritten as follows:

$$k_{\mathrm{C}}\left(\frac{E}{n}\right) n_{\mathrm{e}}(\vec{r}, t) \propto \frac{\mathrm{d}I_{\mathrm{C}}(\vec{r}, t)}{\mathrm{d}t} + \frac{I_{\mathrm{C}}(\vec{r}, t)}{\tau_{\mathrm{eff}}^{\mathrm{C}}}. \tag{8}$$

Equation (8) describes the non-uniform radiation kinetics within the MD channel for the spectral band being considered. Thus, the relative spatio-temporally resolved development of the quantity $k_{\mathrm{C}}(E/n) \cdot n_{\mathrm{e}}$, the so-called excitation rate of the state $\mathrm{N_2}(C\,^3\Pi_{\mathrm{u}})_{\upsilon'=0}$, can be determined from the experimental results in figure 3. In [5] the values of $E/n(z, t)$ were determined in synthetic air by calculating the rate of the excitation rates of two different molecular states (namely $\mathrm{N_2}(C\,^3\Pi_{\mathrm{u}})_{\upsilon'=0}$ and $\mathrm{N_2^+}(B\,^2\Sigma_{\mathrm{u}}^+)_{\upsilon'=0}$). Up to now this analysis has not been possible for axially and radially resolved MD development because the intensity evolution of the (0–0) transition of the FNS (equation (2)) $I_{\mathrm{B}}(r, z, t)$ could not be measured two-dimensionally resolved. Due to the small intensity of the corresponding spectral line at $\lambda_{\mathrm{B}} = 391$ nm the total accumulation time required for measurement of a complete array of data of $I_{\mathrm{B}}(r, z, t)$ exceeds the time of stabilized MD operation. Nevertheless, the qualitative evolution of the excitation rate $k_{\mathrm{C}}(E/n) \cdot n_{\mathrm{e}}$ can be calculated using relation (8). The result of this analysis is shown in figure 5 and compared with the measured intensity for relevant moments.

In the spatio-temporally resolved development of the excitation rate the same subsequent phases of the MD evolution can be seen. As shown in [5], two active zones of MD activity exist. Since the intensity is deconvoluted with the effective lifetime of the radiating state, τ_{eff}, the subsequent phases develop faster and a misalignment between the two series of pictures is seen. For illustration, at $t = 18.7$ ns the maximum of radiation of the investigated spectral transition is observed. But, in contrast, the excitation rate in the discharge gap is about 10% of its highest value (compare figure 5). Furthermore the radial, outward directed propagation of the local maxima, $I_{\mathrm{C}}(r, t_{\mathrm{max}})$, of the discharge on the surface can be seen clearly.

3.2. Short exposure time photos (ICCD) and surface discharges

In figure 6, the temporally integrated radially and axially resolved distributions of the MD luminosity obtained by CCS are compared with the pictures taken using the ICCD-camera. Besides streak photography [16, 17], an ICCD-camera is the only diagnostic tool for the investigation of individual MDs [18]. But under the conditions being considered the MDs occurs statistically. Thus, a temporally and spectrally resolved measurement is not possible using the ICCD-camera.

The 'side view' pictures are in good agreement with the corresponding spectrally resolved CCS data, since the radiation of the SPS dominates in the emission spectrum [5]. The pictures of the 'electrode view' (discharge cell turned towards the camera) demonstrate the real (not averaged) complex discharge structure on the surface. As in [3, 17],

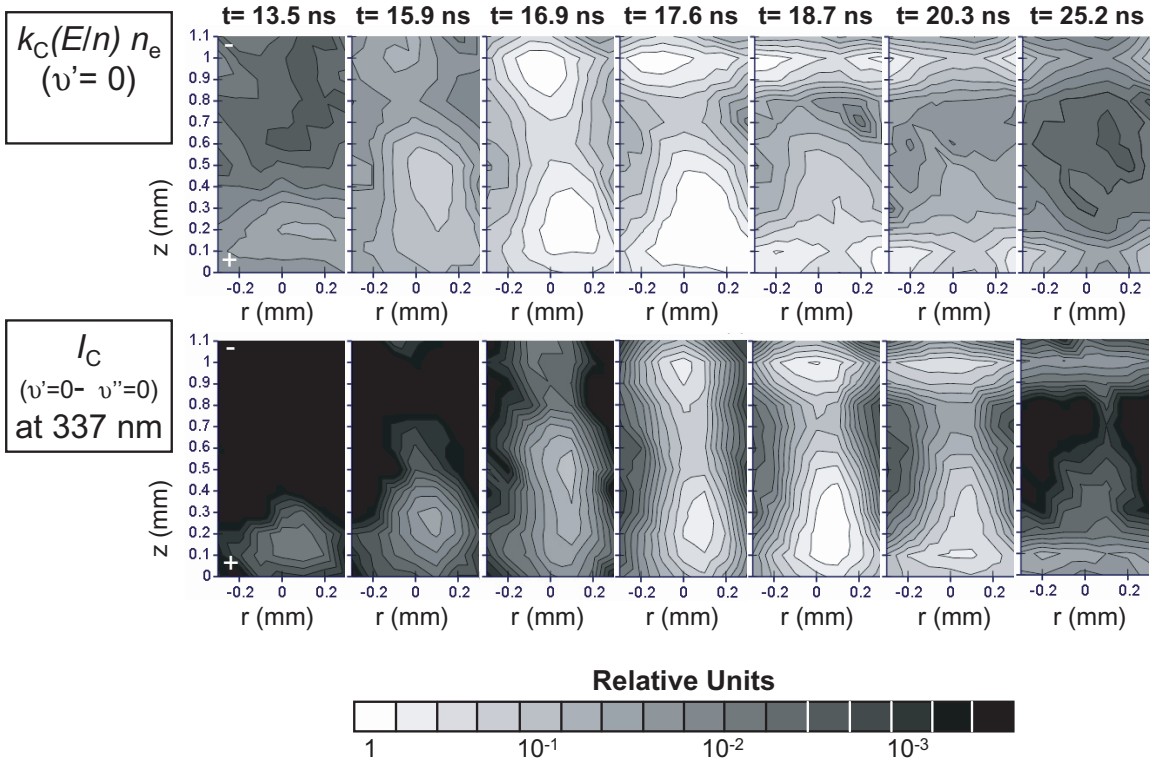

Figure 5. Evolution of the excitation rate, $k_{\mathrm{C}}(E/n(r, z, t)) \cdot n_{\mathrm{e}}(r, z, t)$, of the state $\mathrm{N_2}(C\,^3\Pi_{\mathrm{u}})_{\upsilon'=0}$ within the MD channel (top), compared with the intensity evolution of the SPS, (0–0) transition at $\lambda = 337$ nm (bottom). The system of co-ordinates and electrode polarity are the same as in figure 3.

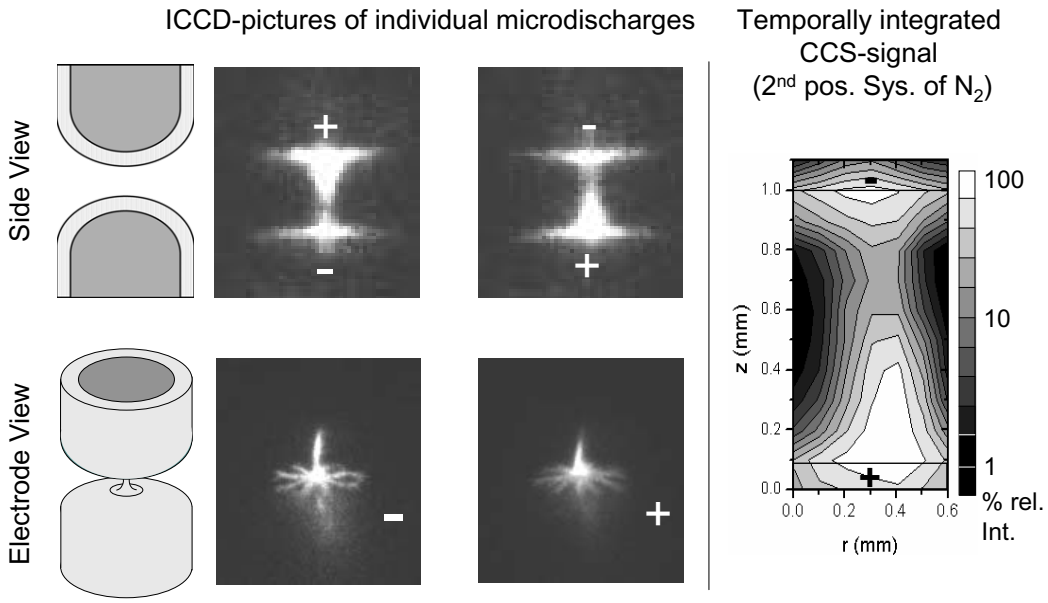

Figure 6. Comparison of the results of short exposure time photography (ICCD) and CCS measurements.

several distinct 'branches' are clearly seen on the cathode. Possibly they are connected to streamer-like discharges propagating on the cathodic dielectric surface [17]. But up to now there is a lack of a detailed understanding of these phenomena. In contrast to earlier investigations [3, 17], the MD footprint on the anode surface appears to be more diffuse, but still with a branched pattern. Similar MD feet were observed in an ac single pulsed corona discharge with the plate electrode covered by glass [19]. A possible explanation for the structure on the anode, shown in figure 6, could be a local field enhancement due to surface charges (positive ions) remaining on the anodic dielectric from the previous MD of opposite polarity. In a discharge configuration with many MDs per half-period of the applied voltage as used in [3, 17], such memory effect may be suppressed by overlapping of the MD feet, and diffuse, funnel-shaped MD feet will be observed. The dielectric material, electrode geometry and frequency of the applied voltage may also play a role.

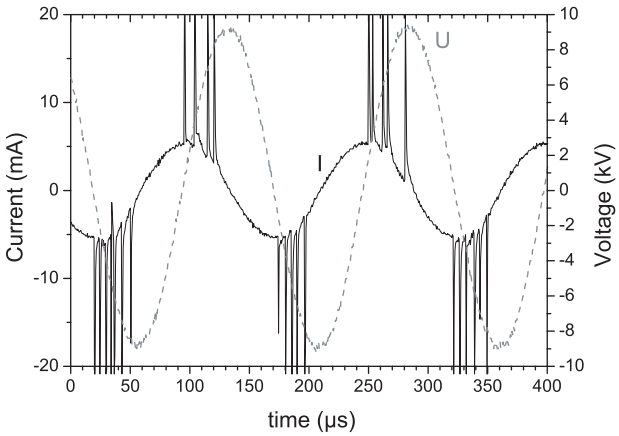

Figure 7. Typical example of the current- and -voltage oscillogram of a BD in air in the case where the feeding voltage amplitude is sufficiently high to provide several MDs per half-period.

3.3. Subsequent microdischarges

An increase in the driving voltage amplitude, U_0, leads to a growth in the number of MDs per voltage half-period, $T/2$. A typical current oscillogram for this situation is shown in figure 7. In the oscillogram the MDs are characterized by the short pulses ('spikes'), overlapping the sinusoidal capacitive (or displacement) current of the BD-cell.

Taking into account the special geometry of the discharge cell (figure 1), it can be expected that in a sequence of MDs during one voltage half-period, the first MD emerges at the position corresponding to the narrowest discharge gap, i.e. between the centres of the electrodes. A further increase in the external voltage provides an electric field which is sufficient for a breakdown in wider gaps, while a second breakdown at the centre is prevented by the remaining surface charges from the first MD. Thus, under the experimental conditions being considered, an increase in U_0 may result in a broadening of the discharge area. To test this hypothesis, a special experiment was carried out. The behaviour of the subsequent MDs studied using the 'direct start–stop' CCS procedure is presented in figure 8.

The first signal in figure 8 at about $t = 0.55\,\mu$s refers to the first MD in a half-period sequence. This MD starts the TAC of the TC-SPC instrument, i.e. it provides the trigger for the CCS measurements. The time interval of the TAC (i.e. the time it waits for the second pulse, the 'stop' pulse of the main signal) was adjusted to $30.4\,\mu$s. Therefore, the spatio-temporal distribution of the luminosity within the range $t = 0.5$–$0.65\,\mu$s (figure 8) corresponds to the spatio-temporal structure of the MDs that are the first ones in the voltage half-period sequences. The following MDs are treated statistically using the CCS method. Therefore the spatio-temporal structure of the luminosity at $t > 4.5\,\mu$s should be interpreted as a distribution function of the MDs over the time axis. The time lag of at least $4\,\mu$s between the first and

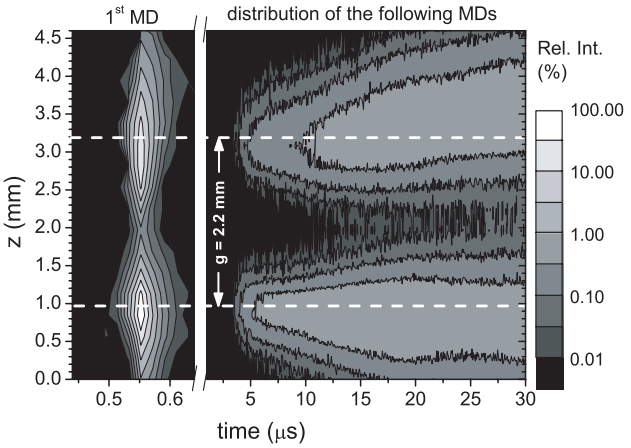

Figure 8. Spatio-temporal distribution of the luminosity of a BD in air ($U_0 = 16.1\,\mathrm{kV_{pp}}$, $f = 5\,\mathrm{kHz}$, $g = 2.2\,\mathrm{mm}$, $\lambda_C = 337\,\mathrm{nm}$) recorded by the CCS instrument operating in a 'direct-start–stop' mode. See text for details.

the second spatio-temporal luminosity distributions in figure 8 correspond to the minimum interval between the first and the second MDs in a half-period sequence. The maxima of the second distribution are broadening and moving in opposite directions outwards from the gap centre. Taking into account the curvature of the electrodes, this movement means a radial extension of the discharge and it is an evidence of the discharge area broadening as described above. The mechanism of this radial extension of the BD implies a key role of the surface charges in determining the distribution of the subsequent MDs over the dielectrics.

4. Summary and outlook

The evolution of the axially and radially resolved structure of the MDs in a BD was studied using CCS and ICCD-camera. For reasons of stability and reproducibility, the axially and radially resolved CCS measurements were only carried out in a gas mixture consisting of 6 vol% O_2 and 94 vol% N_2. The basic phases of the MD development were interpreted in terms of spatially two-dimensional evolution of the electric field and the effects of surface charges, accumulated on the dielectric electrodes. It is shown that the discharges on surfaces develop simultaneously within a nanosecond time range. Due to residual surface charges on the dielectrics, the subsequent MDs within a voltage half-period are generated at different positions, causing a broadening of the discharge area between two semi-spherical electrodes.

Further improvement of the reproducibility and the long-term stability of the repetitive MDs in order to measure the intensity evolution of the FNS and to determine spatially two-dimensionally resolved development of the reduced electric field strength and the electron density is the plan for future investigations. Therefore changes in the discharge cell geometry will be undertaken. Furthermore the MD development on the dielectrics as well as the interaction processes on the surface and volume shall be investigated.

Acknowledgments

The work was supported by Deutsche Forschungsgemeinschaft, SFB 198 'Kinetics of partially ionized plasmas'. We are grateful to Bert Krames (Greifswald, Germany) for his assistance with the ICCD-camera measurements. Two of the authors (RB and KVK) express their gratitude to the German Academic Exchange Sevice (DAAD) for supporting their research visits to Moscow State University (RB) and to the Ernst-Moritz-Arndt University of Greifswald (KVK).

References

[1] Samoilovich V, Gibalov V and Kozlov K 1997 *Physical Chemistry of the Barrier Discharge* (Düsseldorf: DVS)

[2] Eliasson B and Kogelschatz U 1991 Modelling and applications of silent discharge plasmas *IEEE Trans. Plasma Sci.* **19** 309–23

[3] Gibalov V I and Pietsch G J 2000 The development of dielectric barrier discharge in gas gaps and on surfaces *J. Phys. D: Appl. Phys.* **33** 2618–36

[4] Steinle G, Neundorf D, Hiller W and Petralla M 1999 Two-dimensional simulation of filaments in barrier discharges *J. Phys. D: Appl. Phys.* **32** 1350–56

[5] Kozlov K V, Wagner H-E, Brandenburg R and Michel P 2001 Spatio-temporally resolved spectroscopic diagnostics of the barrier discharge in air at atmospheric pressure *J. Phys. D: Appl. Phys.* **34** 3164–76

[6] Wagner H-E, Brandenburg R, Kozlov K V, Sonnenfeld A, Michel P and Behnke J F 2003 The barrier discharge: basic properties and applications to surface treatment *Vacuum* **71** 417–36

[7] Brandenburg R 2004 Räumlich und zeitlich aufgelöste Untersuchungen an filamentierten und diffusen Barrierenentladungen *Thesis* University of Greifswald, Germany (in German)

[8] Kozlov K V, Brandenburg R, Wagner H-E, Morozov A M and Michel P 2005 Investigation of the filamentary and diffuse mode of barrier discharges in N_2/O_2 mixtures at atmospheric pressure by cross-correlation spectroscopy *J. Phys. D: Appl. Phys.* **38** 518–29

[9] Wagner H-E, Kozlov K V, Brandenburg R and Morozov A M 2004 Spatio-temporally resolved spectroscopic diagnostics of the barrier discharge in N_2–O_2 mixtures at atmospheric pressure *Gaseous Dielectrics X* ed L G Chrisophorou *et al* (New York: Springer) pp 77–86

[10] Brandenburg R, Kozlov K V, Morozov A M, Wagner H-E and Michel P 2003 Behavior of dielectric barrier discharges in nitrogen/oxygen mixtures *Proc. 26th Int. Conf. on Phenomena in Ionized Gases (ICPIG-26), (Greifswald, Germany)* vol 4, pp 43–4

[11] Kozlov K V, Dobryakov V V, Monyakin A P, Samoilovich V G, Shepeliuk O S, Wagner H-E, Brandenburg R and Michel P 2002 Cross-correlation spectroscopy in investigations of filamentary gas discharges at atmospheric pressure *Selected Research Papers on Spectroscopy of non-equilibrium plasmas at elevated pressures* ed V N Ochkin *Proc. Int. Society for Optical Engineering (SPIE) Washington (USA)* vol 4460, pp 165–76

[12] Matveev A A and Silakov V P 1998 Method of calculation of specific radiant emitting of the bands of 1− and 2+ systems of nitrogen in the non-equilibrium nitrogen–oxygen plasma *Physics and Technology of Electric Power Transmission* ed A F Djakov (Moscow: MPEI) pp 201–18 (in Russian)

[13] Djakov A F, Bobrov Yu K and Yourguelenas Yu V 1999 Mathematical modelling of nitrogen molecular bands radiation in air streamer discharge *Proc. 14th Int. Symp. on*

Plasma Chemistry, (Praha, Czech Republic) vol V, pp 2785–90

[14] Kossyi I A, Kostinsky A Yu, Matveyev A A and Silakov V P 1992 Kinetic scheme of the non-equilibrium discharge in nitrogen–oxygen mixtures *Plasma Sources Sci. Technol.* **1** 207–20

[15] Pancheshnyi S V, Starikovskaia S M and Starikovskii A Yu 2000 Collisional deactivaton of $N_2(C\,^3\Pi_u, \upsilon = 0, 1, 2, 3)$ states by N_2, O_2, H_2 and H_2O molecules *Chem. Phys.* **262** 349–57

[16] Heuser C and Pietsch G 1980 Pre-breakdown phenomena between glass-glass and metal-glass electrodes *Proc. 6th Int. Conf. on Gas Discharges and their Applications (Edinburgh, UK)* pp 98–101

[17] Heuser C 1985 Zur Ozonerzeugung in elektrischen Gasentladungen *Thesis* RWTH Aachen, Germany (in German)

[18] Merbahi M, Sewraj N, Marchal F, Salamero Y and Millet P 2004 Luminescence of argon in a spatially stabilized mono-filamentary dielectric barrier micro-discharge: spectroscopic and kinetic analysis *J. Phys. D: Appl. Phys.* **37** 1664–78

[19] Akishev Y S, Aponin G I, Grushin M E, Karal'nik V B and Trushkin N I 2004 Pin-to-plane DBD in Ar: Co-existence of diffuse and constricted plasma modes on dielectric surface *Proc. 15th Conf. on Gas Discharges and their Applications (Toulouse, France)* vol 1, pp 243–6